Acta Polytechnica **63**(1):36–49, 2023
https://doi.org/10.14311/AP.2023.63.0036

Published by the Czech Technical University in Prague

FEMTOSECOND LASER PROCESSING OF ADVANCED TECHNICAL MATERIALS

Tomáš Primus[a,b,*], Martin Novák[a], Pavel Zeman[a], František Holešovský[b]

[a] *Czech Technical University in Prague, Faculty of Mechanical Engineering, Department of Production Machines and Equipment, Horská 3, 128 00 – Prague 2, Czech Republic*

[b] *Czech Technical University in Prague, Faculty of Mechanical Engineering, Department of Machining, Process Planning and Metrology ,Technická 4, 160 00 – Prague 6, Czech Republic*

[*] corresponding author: T.Primus@rcmt.cvut.cz

Abstract. Ultra-short pulsed laser ablation may be used for high-precision machining with very low thermal influence on the processed materials. Due to this reason, lasers are increasingly used for processing of advanced materials, such as titanium alloys, nickel-based alloys or steel, every year. In this study, four advanced technical materials were analysed and compared under femtosecond laser irradiation with three different wavelengths. The main laser-material interaction parameters were identified, namely the ablation threshold and removal efficiency parameters. Higher removal rates were found for Ti6Al4V alloy with all three harmonic wavelengths. To increase process productivity, a method of increasing the repetition rate and scanning speed was presented. With the maximum repetition rate, the productivity increased five-fold with a similar removed depth and surface quality. Finally, the suitability of the identified parameters with regard to quality and productivity was demonstrated for fabrication of two complex structures – honeycomb and dot – which has the potential to improve friction properties of advanced materials.

Keywords: Femtosecond laser ablation, Ti6Al4V, Inconel 718, AISI 316L, tool steel, surface texture.

1. Introduction

Ultra-fast lasers operating with femtosecond or picosecond pulses have seen a significant development in the last few years [1]. They have become irreplaceable in many industrial sectors, such as electronics [2], material processing [3] or surface structuring and functionalization [3, 4]. The benefits of ultra-fast laser processing include very precise material processing without heat affection and high process control [5]. However, the knowledge of ablation behaviour and laser-matter interaction is crucial before commencing material processing. Basic ablation characteristics include an ablation threshold and removal efficiency [6, 7]. The ablation threshold indicates the minimum fluence needed to start the material ablation [5, 8, 9]. Removal efficiency can be defined as the amount of material removed per time and per energy input [5]. It has been determined that the maximum removal efficiency can be found for e^2 multiple of the threshold fluence [6]. However, a low process productivity, coupled with the high cost of devices, remains a significant limit. There are several approaches to increasing productivity, including both newly developed methods, such as burst mode [10, 11] or multi-beam technique, [12] and more conventional methods, such as optimization of wavelength [2], in-creased repetition rate [2, 13, 14] or changes in the pulse duration [15]. There are fewer studies of conventional methods, even though optimisation of the repetition rate, energy and wavelength can increase the productivity of the ablation process several-fold on an existing laser equipment. In addition, published studies related to laser matter-interaction basics (e.g. [9, 15, 16]) deal with removal rates in nm/pulse or µm/pulse, which can be difficult to use in practical applications. Moreover, a complex comparison of the ablation characteristics for the same laser set-up among advanced materials, such as steel, titanium alloy and nickel-based alloy is absent from the open literature. These selected materials are used in a wide range of applications ranging from automotive, medicine, oil, and chemical industries to aerospace industry [17–19]. A thorough description of an optimisation of wavelength, laser power and repetition rate for maximizing productivity in the available laser system is likewise lacking, despite the fact that this knowledge is necessary for a wider industrial use of ultra-fast lasers.

This paper presents a complex comparison of ablation behaviour with respect to the surface quality of advanced highly-used industrial materials (Ti6Al4V, Inconel 718, tool steel and stainless steel) under femtosecond laser irradiation by using three different wavelengths. The ideal ablation parameters were studied in depth through an increasing repetition rate experiment resulting in an increased process productivity. Finally, the experimentally obtained results were demonstrated in a complex structure production for a possible tribology application.

2. Materials and methods

2.1. Laser set-up

A femtosecond laser source (Ligtcon Carbide CB3-40W) was used for the experiments. This source was integrated into a Master 1 laser micro-machining station with optical paths for three harmonic wavelengths $\lambda = 1030\,\text{nm}$, 515 nm, 343 nm. The laser beam was delivered through galvo-scanners (InteliScan14) and focused with a F-theta lens on the working plane. The main characteristics of the laser set-up and laser source are listed in Table 1.

Laser source	**Lightcon Carbide CB3-40W**
Wavelength λ [nm]	1030 (IH), 515 (IIH), 343 (IIIH)
Power P_{avg} [W]	40 (IH), 20 (IIH), 11 (IIIH)
Repetition rate f [kHz]	200–1000
Pulse duration τ_p	260 fs –10 ps
Beam quality TEM00; M^2	<1.2 (IH)

Table 1. Laser source type used with main parameters.

2.2. Materials

Four technical materials, namely two types of steel, Inconel 718 nickel-based alloy and Ti6Al4V titanium grade 5 alloy, were chosen for this study. A total of one round shape sample with a diameter of 80 mm and thickness of 15 mm from each material was prepared for the experiments. The surface of the samples was finished by grinding and the initial surface roughness was measured using an InfiniteFocus G5 optical microscope. The results of the initial surface roughness measurements are listed in Table 2. The detailed chemical composition of these materials is listed in Table 3 and their physical properties are listed in Table 4.

Material	**Ra [µm]**	**Rz [µm]**
Tool steel	0.36	3.04
Inconel 718	0.26	2.25
Ti6Al4V	0.40	2.87
Stainless steel	0.40	3.03

Table 2. Initial surface roughness of the samples measured by an optical method according to ISO 25178 standard explained by the parameter Sa (arithmetical mean height of the area) and Sz (maximum height of the area).

3. Methods

In this paper, the full process chain of laser surface structuring is described for four advanced materials (tool steel, stainless steel, Ti6Al4V and Inconel 718). Firstly, the ablation threshold of all four materials under femtosecond laser irradiation with three different wavelengths was studied. Then, the ablation behaviour by removal rates and volume ablation rate with surface roughness was demonstrated for three harmonics. In the interest of increasing surface structuring productivity, the use of a higher repetition rate and scan speed was demonstrated and evaluated. Finally, the suitability of the obtained parameters was demonstrated on surface structuring of two designed structures (dot and honeycomb). The aim of this study is to directly compare the ablation behaviour of four advanced technical materials under laser irradiation from three different wavelengths and femtosecond pulses. Moreover, the obtained parameters were used to increase structuring productivity and complex surface structure preparation.

3.1. Pre-experiment of hatching angle evaluation

Firstly, the effect of the hatching angle on surface roughness was studied to eliminate the effect of the scanning parameters on material behaviour after the laser ablation process. Hatching angle ($\varphi°$) can be defined as an angle of rotation between each laser scanning passes, see Figure 1. For this experiment, 9 different hatching angles were set according to previous knowledge and results from [25]. The main idea for choosing hatching angles was an appropriate combination of even and odd numbers, prime numbers, and including angles from 15 to 90 degrees. Other laser and scanning parameters were kept constant, based on previous knowledge and consequence to upcoming experiments and can be found in Table 5. This experiment was done on the tool steel material, where squares of 5×5 mm were fabricated by 120 laser passes. After each pass, the hatching angle was rotated by φ.

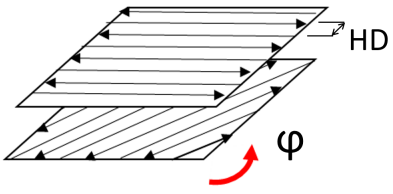

Figure 1. The effect of the hatching angle on surface roughness expressed by Sa [µm].

One of the constant scanning parameters was pulse overlap (S_x), defined as the percentage overlapping of pulses in the beam moving direction. Overlap S_x can be expressed by Equation (1) as the function of the scanning speed v [mm/s], repetition rate f [Hz] and beam diameter 2ω [mm].

Material	Designation	Chemical composition (Wt [%])					
Tool steel	1.2379	C 1.4-1.6	Cr 11-12.5	Mo 0.6-0.9	V 1.2	Mn 0.2-0.4	Si 0.2-0.5
Inconel 718	2.4668	Ni+Co 50-55	Cr 17-21	Mo 2.8-3.3	Ti 0.65-1.15	Al 0.2-0.8	Nb+Ta 4.75-5.5
Ti6Al4V (grade 5)	3.7164	Al 5.5-6.7	V 3.5-4.5	Fe 0-0.4	C <0.08		
Stainless steel (AISI 316L)	1.4404	Cr 16.5-18	Ni 10	Mo 2-2.5	C <0.03		

Table 3. Chemical composition of the samples in Wt [%] and their designation according to DIN norm. Chemical composition data were received from the material supplier.

Material	Melting point [°C]	Density [g/cm³]	Thermal conductivity [W/m K⁻¹]	Thermal expansion coefficient [x10⁻⁶ K]	Ref.
Tool steel	1560	7.6	18.5–20	9.8–12.9	[20]
Inconel 718	1321–1393	8.1	9.3–11.5	8–12	[21, 22]
Ti6Al4V	1660	4.5	6.7–7.3	8.7–9.1	[23]
Stainless steel	1375–1400	7.99	13–17	15–18	[24]

Table 4. The physical properties of tested materials.

Wavelength (λ)	1030 nm
Pulse overlap (Sx)	90 %
Fluence (F)	3.5 J/cm^2
Repetition rate (f)	200 kHz
Square size	5×5 mm
Number of passes	120
Hatching angle (φ)	15°, 17°, 30°, 45°, 53°, 60°, 75°, 83°, 90°

Table 5. Process and scanning parameters used to determine the hatching angle effect on surface roughness.

$$S_x = 1 - \frac{v}{2\omega_0 f} \tag{1}$$

The hatching overlap (H_y) [%] is the percentage overlapping of the hatching lines with a defined hatch distance (HD) and known beam diameter, according to Equation (2). In this study, the same S_x and H_y values were set for all the experiments.

$$H_y = \frac{D - HD}{D} \cdot 100 \tag{2}$$

The surface roughness of the ablated craters was evaluated by the same optical method as the reference state. Parameter Sa [μm] is the arithmetical mean height of the area, an extension parameter of Ra [μm]. Sa values were obtained from measurements of the whole area (5×5 mm) using the Gaussian robust filter according to ISO 25178 [26].

3.2. Ablation thresholds

Different numbers of pulses for ablation threshold determination, varying from 1 to 1000, can be found in the literature [5, 6, 9]. For this experiment, 10 pulses in one place were selected due to the continuity with laser machining with an overlap of 90 %. The ablation threshold evaluation method used in this study, presented, for example, by [6], is based on measuring the crater (spot) diameter. As energy increases, the crater diameter increases, especially for metals. Then, the threshold fluence ($F_{th} = J/cm^2$) and exact spot diameter ($2\omega_0$) can be evaluated using the approximation computation by Equation (3) [6]:

$$\ln 2E_p = \frac{D^2}{2\omega_0^2} + \ln F_{th} + \ln \pi\omega_0^2, \tag{3}$$

where D^2 is the crater diameter for pulse energy E_p. In our case, each selected E_p was repeated ten times in a row and then the crater diameters were measured and averaged to increase the measurement accuracy. For a direct comparison of the ablation behaviour of the selected materials, all three available wavelengths were used.

3.3. Removal efficiency

The removal efficiency experiment was designed using the known ablation threshold values and optimal hatching angle. The main idea of these experiments was to determine the ablation behaviour of the chosen materials, especially the removed volume of material per time. Two different expressions were used for the determination of the ablation efficiency: removal rates $\Delta V/P_{avg}$ [mm^3/min/W] and volume ablation rates

ΔV [mm^3/min] with respect to the surface quality, expressed by the parameter Sa [µm] the arithmetical mean height of the area. Removal rates can be also expressed as a function of fluence threshold (F_{th}) and optical penetration depth δ. Finally, the best values of fluence efficiency were used for the experiment with increasing scanning speed and constant overlap.

$$\frac{\Delta V}{P_{avg}} = \frac{1}{4} \cdot \frac{\delta}{F_{th}} \cdot \ln^2(2 \cdot \frac{F}{F_{th}}) \tag{4}$$

For the removal rate estimations, the squares of 5×5 mm were ablated with 120 laser passes and hatch rotation by a defined angle after each pass. The proper hatching angle was set according to the pre-experimental results. The experiment was performed with a repetition rate of 200 kHz and pulse duration around $\tau \approx 267$ femtoseconds. All of the parameters used in the experiment are presented in Table 6.

λ [nm]	2ω [μm]	S_x, H_y [%]	f [kHz]	τ [fs]
1030 (IH)	33	90	200	267
515 (IIH)	31	90	200	267
343 (IIIH)	22	90	200	267

TABLE 6. Laser and scanning parameters for the removal efficiency experiment.

After laser processing, the samples were cleaned for 15 minutes with ethanol in an ultrasonic bath. The depth and surface roughness of the ablated craters were evaluated with an InfiniteFocus G5 optical microscope (Bruker Alicona, Austria). For detailed observations, a laser confocal microscope VKX-1000 from Keyence was employed.

3.4. Increasing scanning speed and repetition rates

The experimental design that was used for the removal rates was also used for the increasing productivity experiment by increasing the repetition rate with a constant overlap. This experiment was performed for all the materials and for one laser wavelength (1030 nm). The constant parameter of laser fluences found to be the most effective in terms of removal rates was used. Then, the repetition rate was increased from 100 kHz to 1 MHz, with a constant overlap of 90 %, which also resulted in an increase of the scanning speed from 660 to 6600 mm/s. The main idea of this experiment was to determine the highest achievable laser ablation productivity with our laser source.

3.5. Surface structuring

Two structures, namely dot and honeycomb, were designed (Figure 2) to demonstrate the suitability of the identified parameters. The dimensions of each structure are listed in Table 7. For the dot structure, the basic dimensions are the depth (H) and diameter determined by the spot diameter (D) and pitch (R).

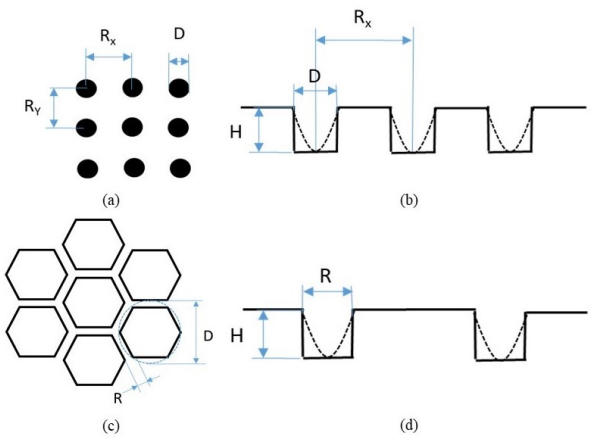

FIGURE 2. Schema of designed surface structures with basic dimension: a) dot structure – view from top; b) dot structure –cros-section profile; c) honeycomb structure – view from top; d) honeycomb structure – cros-section profile.

Structure type	H [µm]	D [µm]	R, Rx, Ry [µm]
Dot	10	35	100
Honeycomb	10	150	35

TABLE 7. Structure dimensions, depth (H), diameter (D), dot pitch (Rx, Ry) and line width of honeycomb structure (R). All values are given in micrometre.

This is the same for the honeycomb structure, where parameter D is defined as the circumscribed circle of one of the hexagons. Pitch (R) for the honeycomb is given by the spot diameter.

4. Results and discussions

4.1. Effect of hatching angle on surface roughness

Before the main experiments, the effect of the hatching angle on surface roughness was estimated. Stainless steel was only one material used for this experiment. The results of the surface roughness measurements for different hatching angles φ obtained from the pre-experiment can be found in Figure 3. The hatching angle $\varphi = 17°$ had the lowest impact on surface roughness and was, therefore, chosen for the subsequent experiments. The highest surface roughness of $Sa = 1.06$ µm was measured for a hatching angle of 45°; it is 1.5 times higher than for an angle of 17°.

4.2. Ablation threshold

The ablation threshold measurement was done for 10 pulses in one place due to the correlation with the following experiments, where an overlap of 90 % was used. Found values are displayed in Figure 4.

The lowest ablation thresholds were generally found for the third harmonics used. This result supports the fact that with decreasing wavelength, photon energy increases [27]. The threshold fluences were found to be

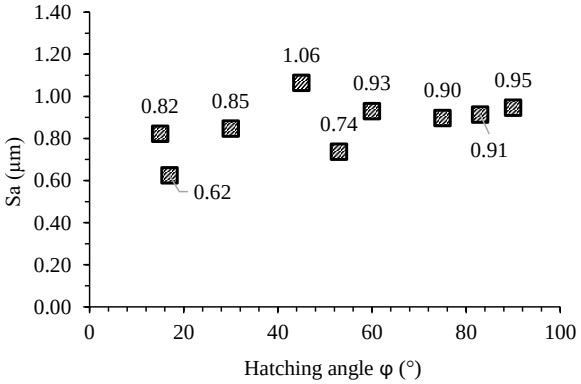

FIGURE 3. The effect of the hatching angle on surface roughness expressed by Sa [µm].

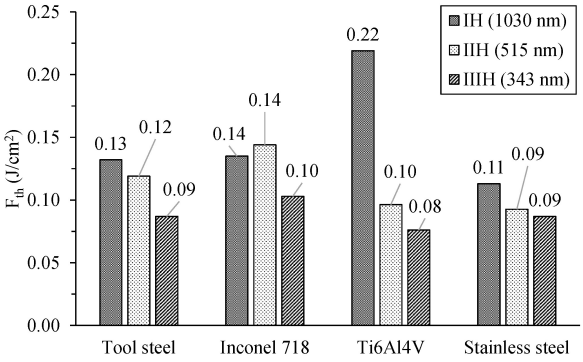

FIGURE 4. The values of ablation threshold for tested materials and wavelengths.

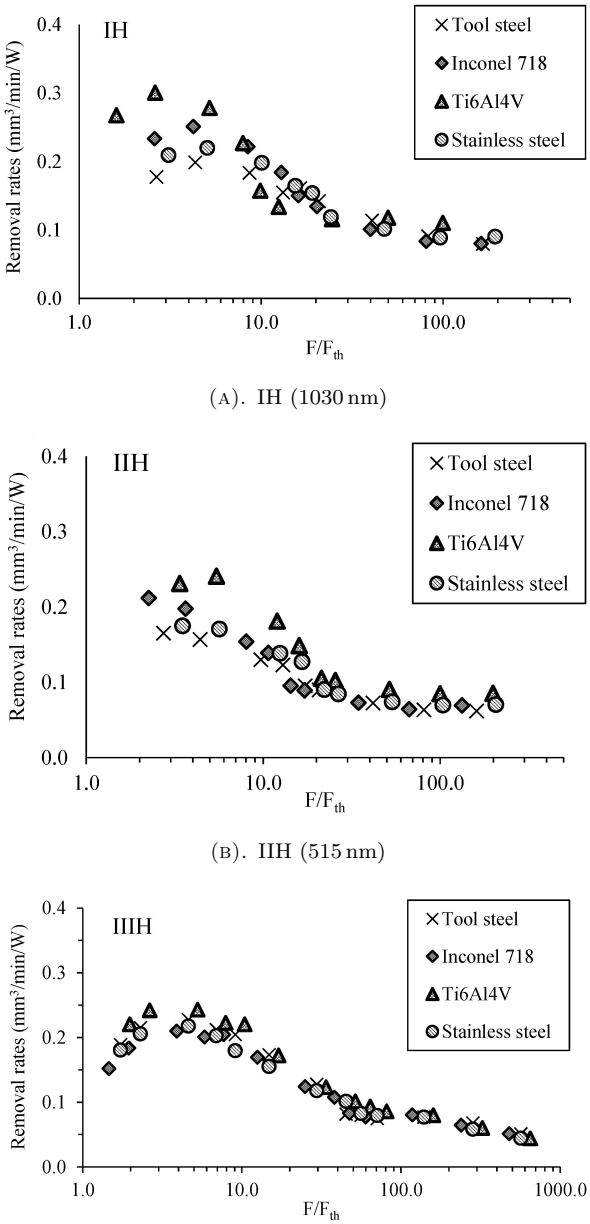

(A). IH (1030 nm)

(B). IIH (515 nm)

(C). IIIH (343 nm)

FIGURE 5. The removal rates for tested materials and three harmonic wavelengths.

similar for all the materials except for Ti6Al4V with the first harmonic, where the highest threshold value of all the materials was measured. Obtained values were compared with the values found in the literature; see Table 8. Mostly the F_{th} for N=1 or N=100 pulses can be found. Similarities between measured and literature values can be seen for F_{th} (100). The threshold for one pulse ablation is usually much higher than for higher pulse counts. The literature review also confirmed that, for the first harmonic used, titanium alloy should have the highest F_{th} of the studied materials.

4.3. Removal efficiency

Using the ablation threshold values, the removal rate dependences were plotted (Figure 5). A logarithmic x-axis with F/F_{th} ratio was used for a better data reproduction. All plot dependences had similar behaviour, reported by [6], reaching a maximum for $e^2 \times F_{th}$, then decreasing and staying constant for a higher F/F_{th} ratio.

The highest removal rates were found for Ti6Al4V titanium alloy for all three harmonics, especially for IH (Figure 5a) where the removal rates reached $\delta V/P_{avg} = 0.3\,\mathrm{mm^3/min/W}$. A possible explanation of this fact may be related to the material's thermal properties. Ti6Al4V titanium alloy had the lowest thermal conductivity (6.7–7.3 $\mathrm{W/m\,K^{-1}}$) of the tested materials. The thermal conductivity coefficient describes the ability of a material to transfer or conduct heat [32]. While, the lowest removal rates were found for tool steel, especially for the optimal F/F_{th} ratio. The thermal conductivity of tool steel is the highest of all the tested materials. The relationship between thermal conductivity and the removal rates is obvious. Even though femtosecond laser irradiation is a cold ablation process, some heat is produced, especially for fluences higher than the ablation threshold. The produced heat is transferred to the lattice. Therefore, for the high thermal conductivity coefficient, a large amount of heat is transferred to the lattice, meaning

Material	Laser wavelength pulse duration	F_{th} (1) [J/cm²]	F_{th} (100) [J/cm²]	Ref.
Ti6Al4V	800 nm, 30 fs	0.29	-	[9]
Ti6Al4V	790 nm, 130 fs	0.272	0.142	[28]
pure Ti	775 nm, 150 fs	0.28	0.08/1.41	[8]
AISI 316L	800 nm, 260 fs	0.21	-	[9]
AISI 304	800 nm, 260 fs	0.24	-	[15]
AISI 316	775 nm, 150 fs	0.21	0.13	[8]
AISI 304	1064 nm, 10 ps	0.5	0.1	[29]
AISI 316	1030 nm 170 fs	0.15	0.135 (50 p)	[14]
AISI 316	1030 nm, 515 nm, 10 ps	0.26 (1030), 0.15 (515 nm)	-	[5]
AISI 304L	800 nm, 100 fs-4,5 ps	0.02-0.05	-	[30]
AISI 304	775 nm, 150 fs	0.16	-	[19]
HR4 nickel alloy, alloy 115	800 nm, 100 s	0.377	0.152	[31]

TABLE 8. Literature review of the fluence threshold values $F_{th}(1)$ and $F_{th}(100)$.

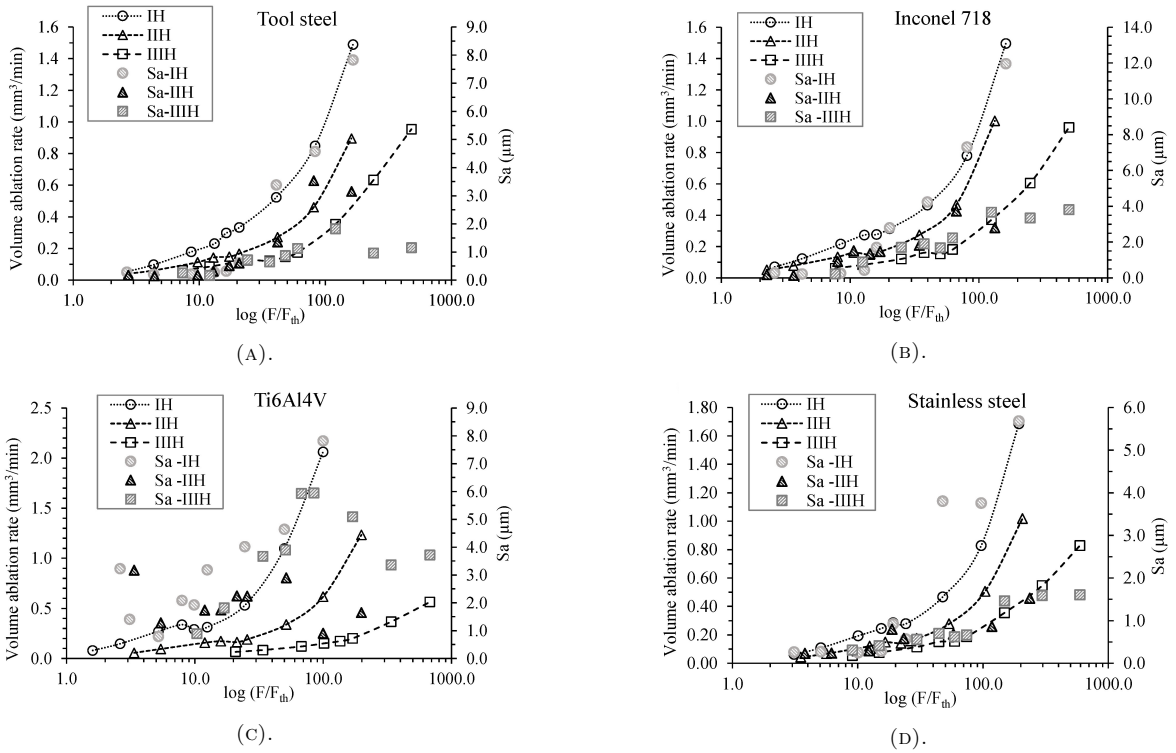

FIGURE 6. Volume ablation rate and surface roughness (Sa) dependency on the laser fluence.

a low amount of heat to melt and ablate the material. As a result, materials with high thermal conductivity are more difficult to ablate by laser.

However, very minor differences in removal rates were found for IIIH (Figure 5c). As reported by [18], material absorptivity, especially for metals, increases with shorter wavelengths. In addition, at shorter wavelengths, the laser energy is absorbed in a smaller volume of material, which localises the heated interaction region. Thus, the possibility of thermal conduction is reduced.

A limit of the removal rate parameter is its focus on process effectivity. In spite of this fact, the volume ablation rate parameter could be useful for describing processes that need higher material ablation without regard to energy consumption. However, negative effects can occur, e.g. heat affection and increased surface roughness. Therefore, a compromise between the ablation rate and surface roughness needs to be found. An ideal example can be seen in Figure 6a for tool steel. For the achieved $\Delta V = 1\,\mathrm{mm}^3/\mathrm{min}$, an ideal solution is to use IIIH, which demonstrated the lowest surface roughness (Sa = 1.1 µm), much lower than for IH (Sa = 4.5 µm) and IIH (Sa = 3.1 µm) for the same volume ablation rate. Similar behaviour was also observed for tool steel (Figure 6a) using IIIH, where Sa remains constant even for higher fluences. For stainless steel (Figure 6d), the Sa values achieved for IIH were lower than for IIIH and much lower than for IH. A very specific behaviour in comparison with the other materials was found for Ti6Al4V (Figure 6c). The lowest Sa was measured for IIH, much lower

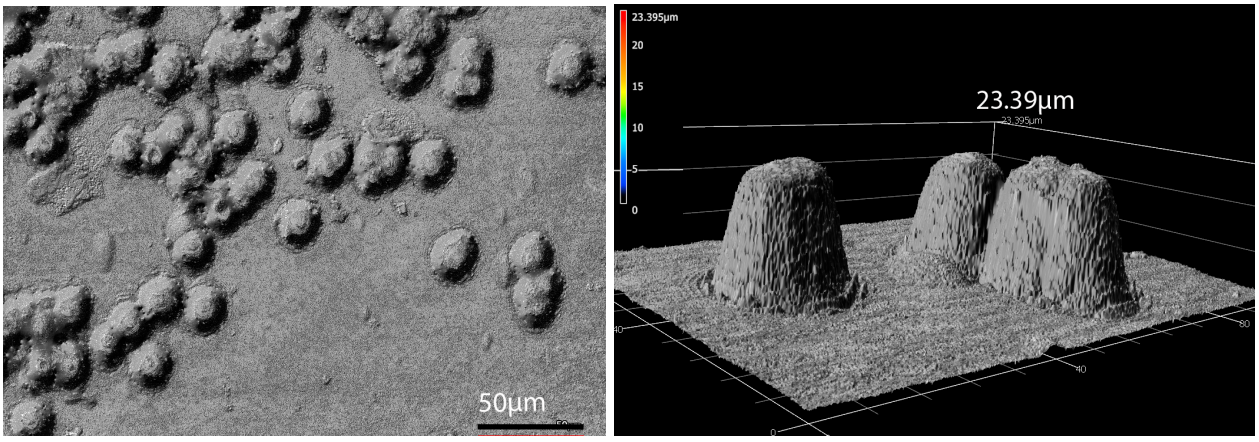

Figure 7. a) 2D image of cone-like features formed on lasered Ti6Al4V surface, b) 3D image of cone-like features.

than for IH and also for IIIH. Moreover, for IIIH, the maximum volume ablation rate was the lowest of all the tested materials. However, for IH, the maximum ($\Delta V = 2.06$ mm^3/min) was achieved in comparison with the other materials, with a very high Sa of 8 µm due to significant thermal effects. High surface melting was observed for all the materials for higher fluences. The highest Sa was measured for Inconel 718, reaching Sa $\approx$ 12 µm.

For Ti6Al4V (Figure 6c), an increase in surface roughness was observed for low fluences, especially for IH and IIH. Optical inspection of ablated areas was done by optical and confocal microscopes. Examples of different ablated materials with same used wavelength and fluence can be seen in Appendix A Figure 11 detailed inspection of the Ti6Al4V surface, for F=0.5 J/cm^2 and IIH used, revealed some debris, see Figure 7. These elements covered the whole lasered surface at a height of about 25 µm. As published by [33], cone-like features form due to material redeposition and the thermal effects of fluences ranging from $F = 0.49$–0.86 J/cm^2. For higher fluences, some micro-cracks start to form. The same results were found in our study. Formation of cone-like features can be limited by using IIIH, probably due to the higher energy of incoming photons along with a higher material absorption.

4.4. Increasing scanning speed and repetition rates

In this paper, the method of increasing the repetition rate for increasing process productivity was chosen. The laser system used allows us to use a 1 MHz repetition rate with a maximum output power of 40 W with a scanning speed of more than 5 m/s. For this reason, the repetition rate was tested across the entire adjustable spectrum from 100 kHz to 1 MHz. The same fluence, which was found to be optimal in the previous experiments, was used, recalculated to the applied repetition rate. The optimal fluence values are shown in Table 9.

Material	F_{opt} **[J/cm^2]**
Stainless steel	0.57
Tool steel	0.57
Inconel 718	0.57
Ti6Al4V	0.45

Table 9. Optimal fluences obtained from removal efficiency experiment for 200 kHz used for increasing scanning speed experiment.

In Figure 8c, the volume ablation rates in relation to the repetition rate are displayed. As expected, the productivity of the process increases by increasing the repetition rate or scanning speed. To demonstrate the inclination of increase, trendlines were used. The highest angle of inclination can be seen for Ti6Al4V. It shows the highest productivity gains. The volume ablation rates increase more than five-fold when the repetition rate is changed from 200 kHz to 1 MHz. However, surface roughness increases slightly for scanning speeds higher than 4000 mm/s (in Figure 8a). This is due to high acceleration and deceleration angles on the short track in combination with the limits of the scanning head that was used. As can be seen from Figure 8b, the removed depth remains constant as the repetition rate and scanning speed increase, respectively. This experiment proved that using a higher repetition rate is beneficial for process productivity. The plots in Figure 8 also demonstrate the ability of the materials to be ablated by laser. The highest removed depth was measured for Ti6Al4V along with the greatest surface roughness caused by significant melting and redeposition of debris as presented for 200 kHz. The steel materials show the lowest removed depth with low surface roughness, comparable to Inconel 718. While, the removed depth was significantly higher for Inconel 718 than for both of the steel materials.

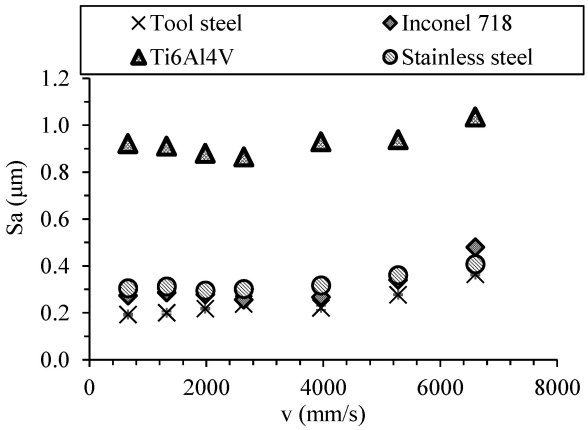

(A). Surface roughness.

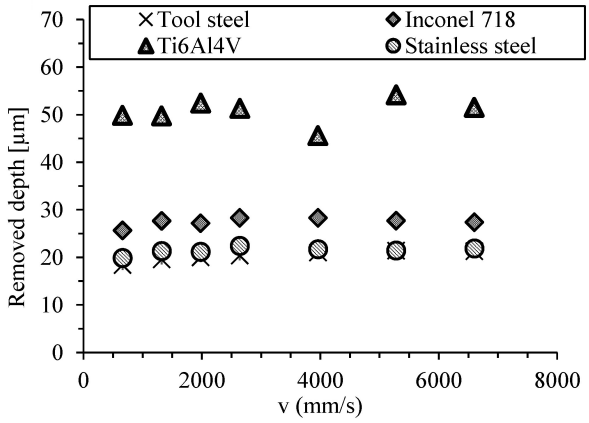

(B). Removed depth.

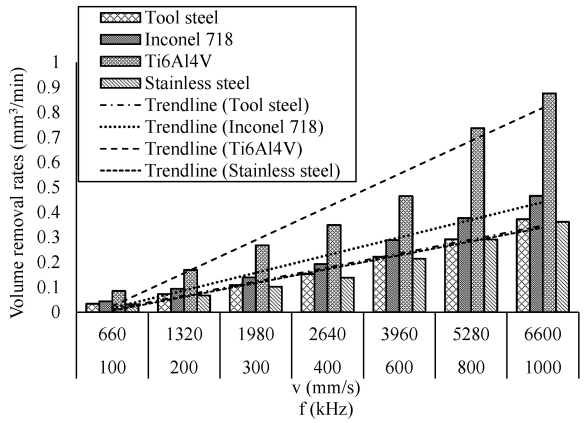

(C). Volume removal rates.

FIGURE 8. Increasing scanning speed results.

4.5. SURFACE STRUCTURING

Using the maximal repetition rate and scanning speed is useful in regard to high process productivity. Some scanning problems can appear during high scanning speeds, such as acceleration and deceleration for short tracks. Even when the sky-writing function developed by galvo-scanner provider SCANLAB GmbH company is used, it is best to use a scanning speed below 4 m/s, especially for geometrically complex structures. The sky-writting function uses predictive algorithms for eliminating acceleration and deceleration of the galvo-scanner mirrors. Two different structures were chosen for the demonstration of the developed processing parameters, namely dot and honeycomb structures. The dot structure was fabricated using a different number of pulses in one place with a defined fluence.

The honeycomb structure was based on a CAD model. The laser beam moved through the lines defined by the model. Both structures had a similar depth of H = 10 µm. The results of the dot structure measurement are presented in the Table 10. Structure depth, diameter and line width were measured from 10 profile lines across the sample. The shape of the fabricated dots was good without material ejection over the edge of the crater. All the dots also had a very good circularity and the proposed depth was achieved. The honeycomb structure also achieved good compliance with the proposed dimensions; see Table 11. A repetition rate of 600 kHz and scanning speed of 3.9 m/s were used for structuring with fluences ranging from $F = 1.27$ to $1.84\,\mathrm{J/cm^2}$ according to the fabricated material. The proposed depth was achieved by a defined number of repetitions ranging from 24 to 28. A very precise structure depth can be obtained with this strategy, with a deviation of only a few tens of micrometre. An example of a 2D view and depth profile of the dot structure for each material can be seen in Appendix A Figure 10 and for the honeycomb structure in Appendix A Figure 11. The designed and fabricated structures have the potential to improve friction properties of materials by decreasing the coefficient of friction as reported by [34]. Structured surfaces can be beneficial in moving mechanical components made from advanced materials such as mechanical seals, piston rings or thrust bearings.

5. CONCLUSIONS

Based on the observations of the current study, the following conclusions can be drawn:

- The ideal hatching angle was found in the pre-experiment. A hatching angle of 17° had the lowest impact on surface roughness. Using odd hatching angles has the advantage that the laser beam never scans twice in the same path.
- The ablation threshold was measured for all the materials using three harmonic wavelengths. The highest fluence threshold value was found for Ti6Al4V titanium alloy when using the first harmonic (1030 nm). Conversely, using the third harmonic (343 nm) led to the lowest ablation thresholds due to the high energy of the incoming photons.
- The highest ablation rates were obtained for Ti6Al4V, especially for IH and IIH, because Ti6Al4V had the lowest thermal conductivity of all the tested materials. For higher F/F_{th} ratio, the differences become smaller. However, the surface roughness expressed by Sa [µm] was the highest of all the materials. Also, some cone-like structures

Material	F [J/cm^2]	Number of pulses [-]	H [µm]	D [µm]
Tool steel	0.573	250	10.37 ± 0.31	28.5 ± 0.77
Inconel 718	0.573	210	10.17 ± 0.23	29 ± 0.73
Ti6Al4V	0.456	180	9.77 ± 0.19	28 ± 0.65
Stainless steel	0.573	260	10.18 ± 0.28	28.4 ± 0.82

Table 10. Laser parameters used for dot structure fabrication with measured results of hole depth (H) and diameter (D).

Material	F [J/cm^2]	Number of pulses [-]	S_x, H_y [%]	H [µm]	R [µm]
Tool steel	1.56	26	90	9.56 ± 0.22	33.5 ± 0.52
Inconel 718	1.56	24	90	9.57 ± 0.25	36 ± 0.65
Ti6Al4V	1.27	24	90	10.14 ± 0.34	31.3 ± 0.47
Stainless steel	1.84	28	90	10.2 ± 0.18	37.1 ± 0.84

Table 11. Laser and scanning parameters used for honeycomb structure fabrication with measured results of structure depth (H) and line width (R).

formed on the lasered surfaces for lower fluences. These effects can be eliminated by using IIIH.

- For IIIH, the differences between the ablation behaviour of all the materials were negligible. For shorter wavelengths, the absorptivity of metals increases and at the same time, the effect of thermal conductivity decreases.
- The experiment for increasing productivity was successful. It was proved that the productivity can be increased more than five-fold. At the same time, a higher scanning speed did not have a negative effect on the surface roughness or removed depth.
- A demonstration of the identified parameters was presented in fabrication of two different complex structures. Good shape and circularity were obtained for the dot structure, along with compliance with the proposed depth of the structure. Simultaneously, the honeycomb structure was fabricated according to the proposal with a good optical quality. Both structures had the potential to improve friction properties of advanced materials.

The presented study summarises and compares the ablation behaviour of four advanced materials and gives a complete overview of the findings of basic ablation parameters for a complex shape structure production by femtosecond laser.

List of symbols

λ Wavelength [nm]
F Fluence [J/cm^2]
F_{th} Threshold fluence [J/cm^2]
E_p Pulse energy [J]
τ Pulse duration [ps, fs]
f Repetition rate [kHz]
M^2 Laser beam quality [–]
S_x Pulse overlap in scanning direction [%]
H_y Pulse overlap in traverse direction [%]
φ Hatching angle [°]
δ Optical penetration depth [nm]

Acknowledgements

This work was supported by the Grant Agency of the Czech Technical University in Prague, grant no. SGS22/159/OHK2/3T/12 and no. SGS22/158/OHK2/3T/12.

References

[1] K. Sugioka. Progress in ultrafast laser processing and future prospects. *Nanophotonics* **6**(2):393–413, 2017. https://doi.org/10.1515/nanoph-2016-0004.

[2] N. Hodgson, A. Steinkopff, S. Heming, et al. Ultrafast laser machining: process optimization and applications. *Laser Applications in Microelectronic and Optoelectronic Manufacturing (LAMOM) XXVI* **11673**:1167308, 2021. https://doi.org/10.1117/12.2584178.

[3] K. Ahmmed, C. Grambow, A.-M. Kietzig. Fabrication of micro/nano structures on metals by femtosecond laser micromachining. *Micromachines* **5**(4):1219–1253, 2014. https://doi.org/10.3390/mi5041219.

[4] J. Bonse, S. Kirner, M. Griepentrog, et al. Femtosecond laser texturing of surfaces for tribological applications. *Materials* **11**(5):801, 2018. https://doi.org/10.3390/ma11050801.

[5] P. Lickschat, D. Metzner, S. Weißmantel. Fundamental investigations of ultrashort pulsed laser ablation on stainless steel and cemented tungsten carbide. *The International Journal of Advanced Manufacturing Technology* **109**(3-4):1167–1175, 2020. https://doi.org/10.1007/s00170-020-05502-8.

[6] B. Jaeggi, B. Neuenschwander, M. Schmid, et al. Influence of the pulse duration in the ps-regime on the ablation efficiency of metals. *Physics Procedia* **12**:164–171, 2011. https://doi.org/10.1016/j.phpro.2011.03.118.

[7] V. Stankevič, A. Čermák, S. Mikalauskas, et al. Processing of ultra-hard materials with picosecond pulses: From research work to industrial applications. *Journal of Laser Applications* **30**(3):032202, 2018. https://doi.org/10.2351/1.5040633.

[8] P. Mannion, J. Magee, E. Coyne, et al. The effect of damage accumulation behaviour on ablation thresholds and damage morphology in ultrafast laser micro-machining of common metals in air. *Applied Surface Science* **233**(1-4):275–287, 2004. https://doi.org/10.1016/j.apsusc.2004.03.229.

[9] S. Xu, Y. Chen, H. Liu, et al. Femtosecond laser ablation of Ti alloy and Al alloy. *Optik* **212**:164628, 2020. https://doi.org/10.1016/j.ijleo.2020.164628.

[10] P. Lickschat, A. Demba, S. Weissmantel. Ablation of steel using picosecond laser pulses in burst mode. *Applied Physics A* **123**(2):123–137, 2017. https://doi.org/10.1007/s00339-016-0743-y.

[11] M. Domke, V. Matylitsky, S. Stroj. Surface ablation efficiency and quality of fs lasers in single-pulse mode, fs lasers in burst mode, and ns lasers. *Applied Surface Science* **505**:144594, 2020. https://doi.org/10.1016/j.apsusc.2019.144594.

[12] P. Hauschwitz, R. Bičštová, A. Brodsky, et al. Towards rapid fabrication of superhydrophobic surfaces by multi-beam nanostructuring with 40,401 beams. *Nanomaterials* **11**(8), 2021. https://doi.org/10.3390/nano11081987.

[13] J. Finger, C. Kalupka, M. Reininghaus. High power ultra-short pulse laser ablation of IN718 using high repetition rates. *Journal of Materials Processing Technology* **226**:221–227, 2015. https://doi.org/10.1016/j.jmatprotec.2015.07.014.

[14] J. Schille, A. Heisterkamp, J. Neev, et al. High repetition rate femtosecond laser processing of metals. *Proceedings SPIE: Ultrafast Optics: Biomedical, Scientific, and Industrial Applications X* **7589**:758915, 2010. https://doi.org/10.1117/12.842600.

[15] S. Xu, R. Ding, C. Yao, et al. Effects of pulse durations and environments on femtosecond laser ablation of stainless steel. *Applied Physics A* **124**:310, 2018. https://doi.org/10.1007/s00339-018-1714-2.

[16] X. Sedao, M. Lenci, A. Rudenko, et al. Influence of pulse repetition rate on morphology and material removal rate of ultrafast laser ablated metallic surfaces. *Optics and Lasers in Engineering* **116**:68–74, 2019. https://doi.org/10.1016/j.optlaseng.2018.12.009.

[17] G. Çam, G. İpekoğlu, K.-H. Bohm, M. Koçak. Investigation into the microstructure and mechanical properties of diffusion bonded TiAl alloys. *Journal of Materials Science* **41**(16):5273–5282, 2006. https://doi.org/10.1007/s10853-006-0292-4.

[18] M. Henry, P. M. Harrison, I. Henderson, et al. Laser milling: a practical industrial solution for machining a wide variety of materials. *Proceedings of the SPIE* **5662**:627–632, 2004. https://doi.org/10.1117/12.596743.

[19] P. Mannion, T. J. Glynn, J. Magee, et al. Ablation thresholds in ultrafast laser micromachining of common metals in air. *Proceedings SPIE: Opto-Ireland 2002: Optics and Photonics Technologies and Applications* **4876**:470–478, 2003. https://doi.org/10.1117/12.463744.

[20] HASCO company. Material characteristics – 1.2379. [2022-08-04], https://www.hasco.com/en/werkstoffdatenblatt_1.2379.

[21] A. S. Hakeem, F. Patel, N. Minhas, et al. Comparative evaluation of thermal and mechanical properties of nickel alloy 718 prepared using selective laser melting, spark plasma sintering, and casting methods. *Journal of Materials Research and Technology* **12**:870–881, 2021. https://doi.org/10.1016/j.jmrt.2021.03.043.

[22] NeoNickel. (2021) Data sheet – alloy 718. [2022-08-04], https://www.neonickel.com/alloys/nickel-alloys/alloy-718/.

[23] Material-properties.org. (2022) About grade 5 titanium alloy – Ti-6Al-4V. [2022-08-04], https://material-properties.org/ti-6al-4v-density-strength-hardness-melting-point/.

[24] AZoNetwork. (2001) AZo materials, stainless steel – Grade 316 (UNS S31600), datasheet. [2022-08-04], https://www.azom.com/properties.aspx?ArticleID=863.

[25] C. Daniel, J. Manderla, S. Hallmann, C. Emmelmann. Influence of an angular hatching exposure strategy on the surface roughness during picosecond laser ablation of hard materials. *Physics Procedia* **83**:135–146, 2016. https://doi.org/10.1016/j.phpro.2016.08.026.

[26] International Organization for Standardization. *ISO 25178-2:2021, Geometrical product specifications (GPS) – Surface texture: Areal – Part 2: Terms, definitions and surface texture parameters, second edition*, 2021.

[27] M. D. Shirk, P. A. Molian. A review of ultrashort pulsed laser ablation of materials. *Journal of Laser Applications* **10**(1):18–28, 1998. https://doi.org/10.2351/1.521827.

[28] N. Maharjan, W. Zhou, Y. Zhou, Y. Guan. Ablation morphology and ablation threshold of Ti-6Al-4V alloy during femtosecond laser processing. *Applied Physics A* **124**(8):519, 2018. https://doi.org/10.1007/s00339-018-1928-3.

[29] G. Raciukaitis, C. R. Phipps, M. Brikas, et al. Accumulation effects in laser ablation of metals with high-repetition-rate lasers. *Proceedings SPIE: High-Power Laser Ablation VII* **7005**:70052L, 2008. https://doi.org/10.1117/12.782937.

[30] R. Le Harzic, D. Breitling, M. Weikert, et al. Pulse width and energy influence on laser micromachining of metals in a range of 100fs to 5ps. *Applied Surface Science* **249**(1-4):322–331, 2005. https://doi.org/10.1016/j.apsusc.2004.12.027.

[31] T. L. See, Z. Liu, H. Liu, et al. Effect of geometry measurements on characteristics of femtosecond laser ablation of HR4 nickel alloy. *Optics and Lasers in Engineering* **64**:71–78, 2015. https://doi.org/10.1016/j.optlaseng.2014.07.011.

[32] Z. Pluta, T. Hryniewicz. Thermal expansion of solids. *Journal of Modern Physics* **3**(8):793–802, 2012. https://doi.org/10.4236/jmp.2012.38104.

[33] G. Schnell, H. Lund, S. Bartling, et al. Heat accumulation during femtosecond laser treatment at high repetition rate – a morphological, chemical and crystallographic characterization of self-organized structures on Ti6Al4V. *Applied Surface Science* **570**:151115, 2021. https://doi.org/10.1016/j.apsusc.2021.151115.

[34] M. Bieda, C. Schmädicke, T. Roch, A. Lasagni. Ultra-low friction on 100Cr6-steel surfaces after direct laser interference patterning. *Advanced Engineering Materials* **17**(1):102–108, 2015. https://doi.org/10.1002/adem.201400007.

A. Appendices

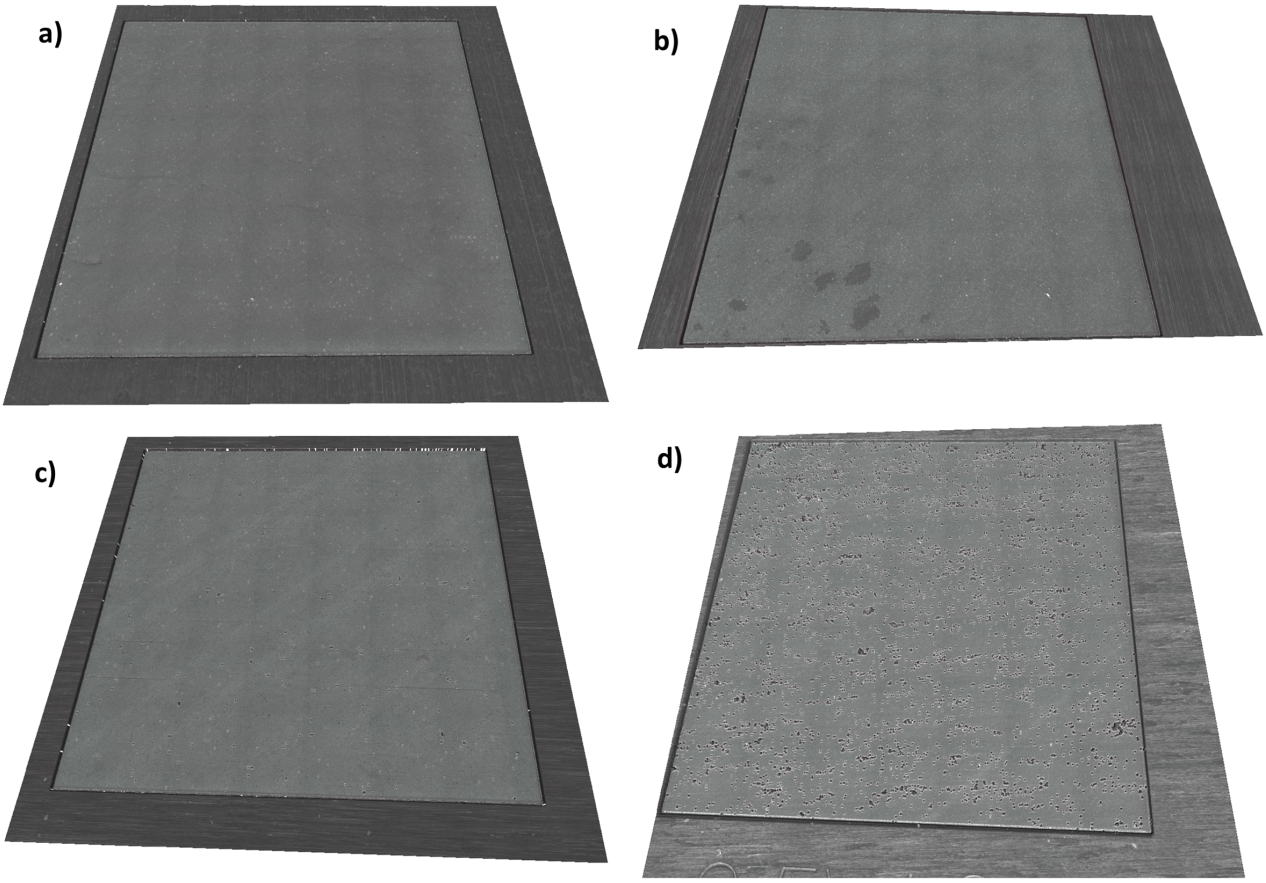

Figure 9. 3D images of ablated materials a) tool steel; b) stainless steel; c) Inconel 718; d) Ti6Al4V, using IIH and $F = 0.52\,\mathrm{J/cm^2}$.

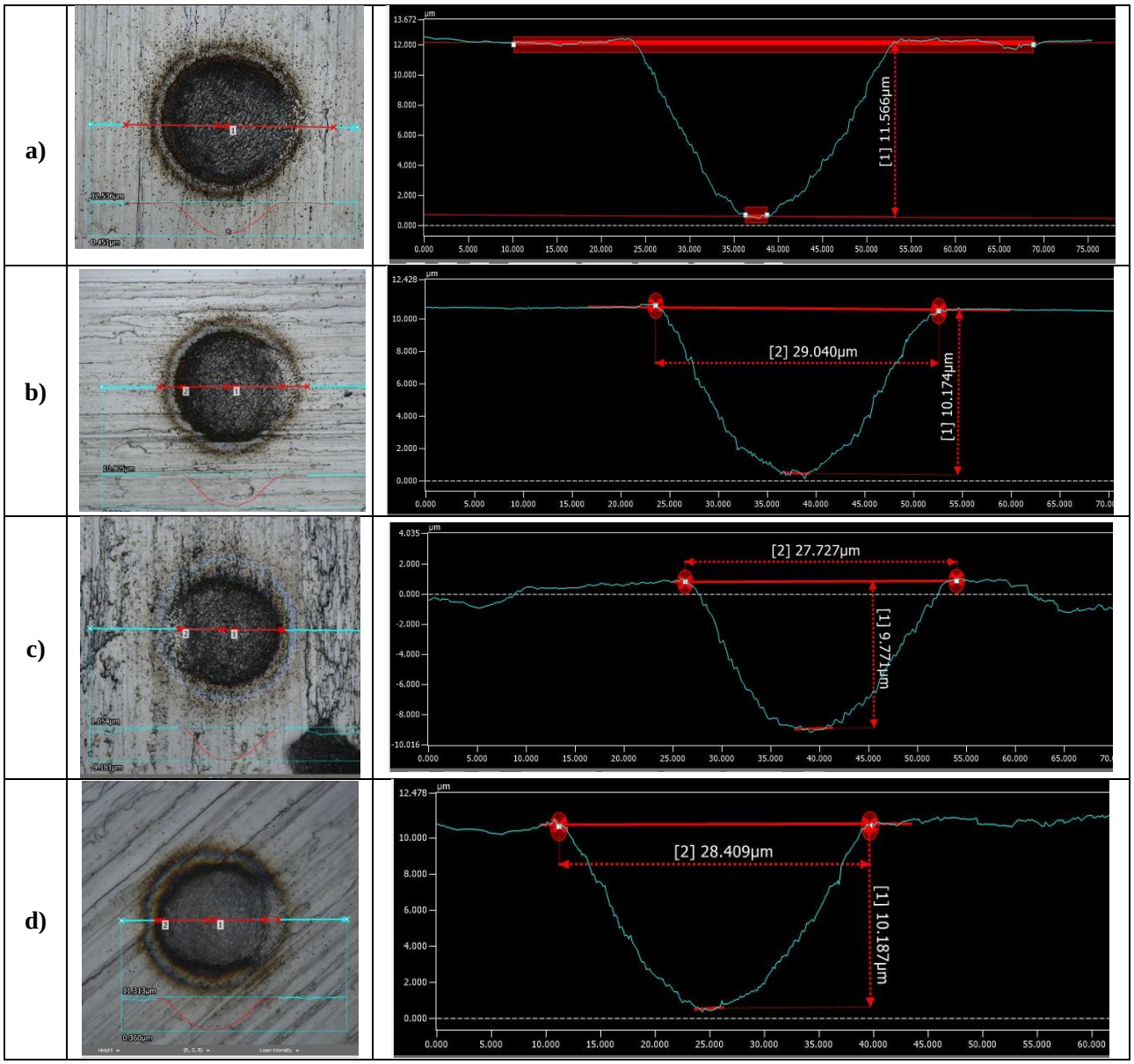

FIGURE 10. Examples of the dot structure fabricated in the tested materials: left – 2D image, right – depth profile, a) Tool steel; b) Inconel 718; c) Ti6Al4V; d) Stainless steel.

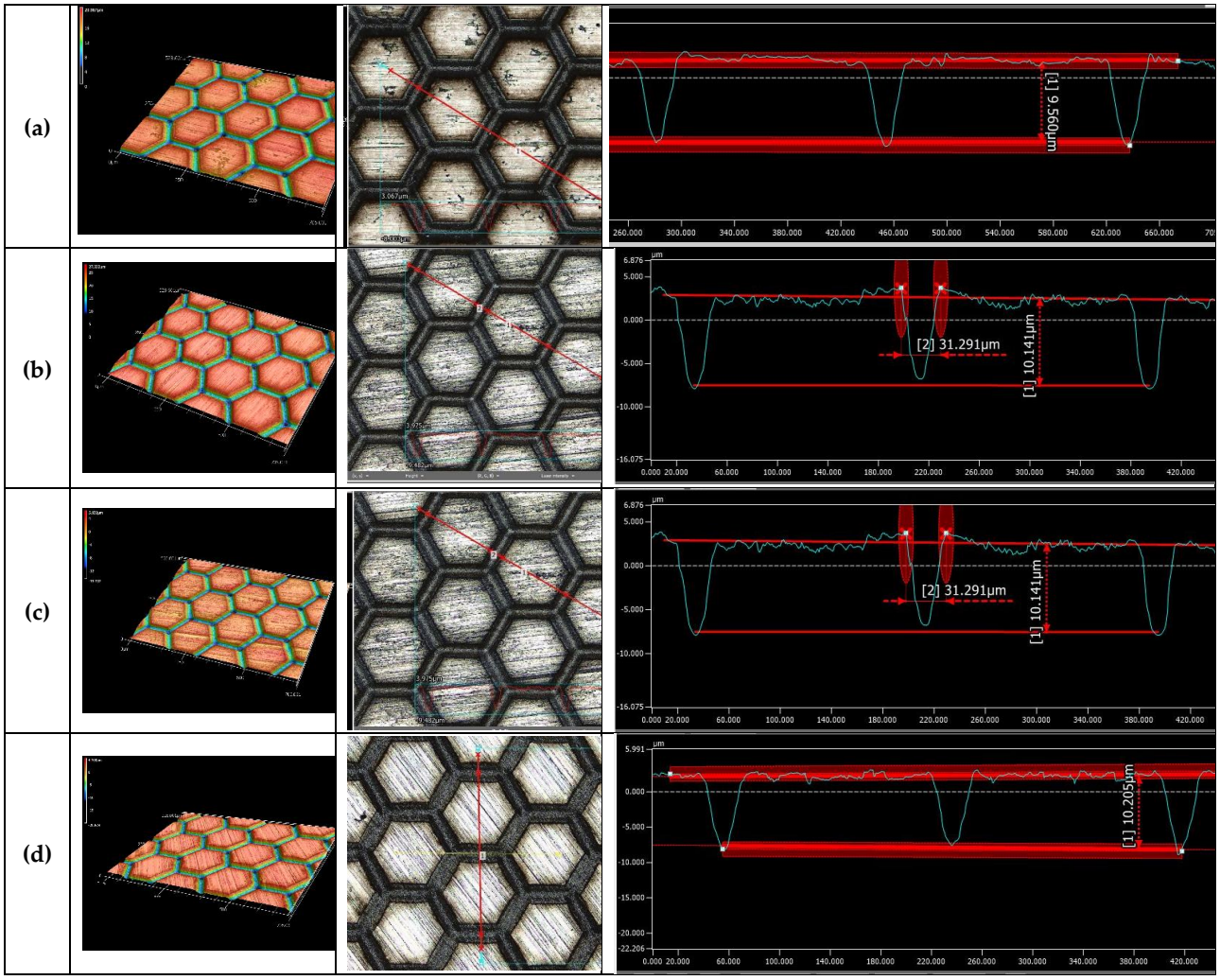

FIGURE 11. Examples of the honeycomb structure fabricated in the tested materials: left – 3D image, right – depth profile, a) Tool steel; b) Inconel 718; c) Ti6Al4V; d) Stainless steel.